Effect of Crater Formation on the Absorption of Focused Laser Light

C. Randall and J. S. DeGroot
University of California, Lawrence Livermore Laboratory, Livermore, California 94550, and Department of Applied Science, University of California, Davis, California 95616
(Received 11 April 1978)

We use a new computational model to investigate the absorption of a focused beam of circularly polarized laser light, including the ponderomotive force. We find, in agreement with recent experiments, that at high intensity large craters can form due to the variation of the ponderomotive force across the focal region. The critical surface becomes concave and the walls of the crater refract the incident light so that resonant absorption can be greatly enhanced.

Resonant absorption of laser light is thought to be the dominant heating mechanism for plasmas irradiated by high-power lasers. To date most theoretical and computational studies of resonant absorption have approximated the incident laser beam as a plane wave.[1,2] The present paper indicates that if the effects of a finite focused laser beam are taken into account, then the absorption may be greatly increased over the plane-wave value.

In particular, recent experiments[3] on the absorption of high-intensity laser light indicate that large-scale craters may form in the underdense plasma. These craters are not present at low intensities and their dimensions correspond to the laser spot size, confirming the role of radiation pressure in their formation. They arise because self-steepening of the plasma density takes place preferentially near the center of the focal spot, indenting the critical surface where the beam is most intense. In addition, the outward flow from the ablation region is restricted by the light pressure so that the plasma is forced to expand around the laser beam. Large-scale cratering arising from a finite focal spot occurs in addition to the small-scale rippling of the critical surface due to instabilities. Such critical surface instabilities are operative even for planar incident light and have been reported elsewhere.[4]

Experiments[5,6] also indicate that some mechanism is acting to smooth out the sharp angle and polarization dependence of absorption suggested by particle simulations which use planar light. While many alternative explanations exist (notably megagauss d.c. magnetic fields[7,8] and ion acoustic turbulence[9,10]) large craters seem to be important in this regard. Associated with craters are a concave critical surface and strong transverse density gradients in the underdense region, which significantly refract the incoming light. Both features increase the effective angle of incidence of light so that resonant absorption is enhanced. Even for apparent normal incidence fractional absorption may be in the range of (30–45)%, as compared with 15% in the absence of crater formation.

We have developed a computational model to study craters formed by focused laser beams, their stability, and their consequences for absorption. It includes wave-optics solutions for arbitrarily focused light, a description for resonant absorption, and an isothermal hydrodynamic description of the plasma response to the pondermotive force.

For a linearly polarized focused laser beam the ponderomotive force in inherently three dimensional[11] as a result of polarization-dependent (resonant) absorption. However, we find a numerically tractable, self-consistent approximation to the problem by assuming a circularly polarized incident beam. In that case the ponderomotive force and hence the plasma density profile are azimuthally symmetric about the laser axis.[12] Aside from some small-scale modulations in the azimuthal direction due to critical surface and/or underdense plasma instabilities, the plasma density will share this symmetry. However, small azimuthal density modulations are probably unimportant for the formation of focal-spot–sized craters. We neglect them and assume a plasma density profile which is rigorously azimuthally symmetric.

We describe the propagation of the laser light with the equation

$$\frac{\partial^2 \vec{E}}{\partial t^2} + \nu \frac{\partial \vec{E}}{\partial t} = c^2 \nabla \times \nabla \times \vec{E} - \omega_p^2 \vec{E} - v_e^2 [\gamma \nabla (\nabla \cdot \vec{E}) - (\nabla \cdot \vec{E}) \nabla n_0 / n_0] + \nabla \sigma \left(\nabla \cdot \frac{\partial \vec{E}}{\partial t} \right), \quad (1)$$

where n_0 is the background plasma density, ν is the collisional damping rate, γ is the ratio of specific heats, $\omega_{pe}^2 = 4\pi ne^2/m$, v_e is the electron thermal velocity, $v_e^2 = T_e/m$, and σ is a phenomenological "diffusion coefficient" for charge density. When $\sigma = 0$, Eq. (1) is the familiar linearized electric-field wave equation. At low intensities it predicts resonant absorption field intensities and absorption coefficients in good agreement with particle simulations.[1] At higher intensities direct heating of electrons results in a large nonlinear dissipation not included in this linear equation. As a result, the longitudinal fields are overestimated. Because these fields often dominate the ponderomotive force and hence the plasma hydrodynamic response, it is important to improve this description. This is done by giving a nonlinear dependence on the electric field strength:

$$\sigma = \sigma_{NL}(|\nabla \cdot \vec{E}|/4\pi n_0 e)^{\alpha}, \tag{2}$$

where σ_{NL} and α are positive constants. For $\alpha \geq 2$ the fluctuating plasma density is effectively limited to $\delta n/n \leq 1$ since the damping grows extremely heavy for larger values. This is exactly the behavior required to model cold wave breaking.[2] We have verified numerically that the calculated absorption is independent of the parameters σ_{NL} and α for fixed density profiles. In practice we exploit this independence and choose σ_{NL} and α to give self-steepened density-profile scale lengths of $(10-20)\lambda_D$ in agreement with particle simulations.

We solve Eq. (1) in a spherical (r, θ, φ) coordinate system oriented along the laser axis. For circularly polarized light and an azimuthally symmetric plasma it is appropriate to remove the azimuthal dependence of the fields as $e^{i\varphi}$. Then Eq. (1) is effectively two dimensional and may be differenced on an r-θ grid. The time advancement is done explicitly and the fields on the vacuum boundary are obtained by an adaption of Lindman's[13] scheme to spherical coordinates.

The plasma dynamics are followed by solving the isothermal fluid equations:

$$\frac{\partial n}{\partial t} + \nabla \cdot (n\vec{v}) = 0, \tag{3a}$$

$$M\left(\frac{\partial}{\partial t}(n\vec{v}) + \nabla \cdot (n\vec{v}\vec{v})\right) = -T\nabla n - \frac{ne^2}{2m\omega_0^2}\nabla\langle E^2\rangle + \nabla \cdot (\vec{\mu} \cdot \nabla\vec{v}), \tag{3b}$$

where m, n, and $\vec{v}$ are the ion mass, plasma density, and plasma velocity, respectively, and T is the thermal electron temperature. The assumption that the thermal electrons are isothermal is consistent with particle simulations. The artificial viscosity tensor $\vec{\mu}$ is the standard Von Neumann formulation to which we have added a second contribution which is a constant in space, and which is used to simulate Landau damping of ion waves. The angular brackets, $\langle\rangle$, in the ponderomotive force driving term denote a time average over the laser period $2\pi/\omega_0$. The fluid equations are advanced once per laser cycle by the conservative Lax-Wendroff algorithm. Because our equations are solved on the ω_0 time scale, we use an artificial electron-ion mass ratio, typically, 0.01.

In the following example calculation we model the conditions of the high-intensity, short-pulse-length disk experiments[5] referred to above. We consider the situation where a crater has been formed during the early part of the laser pulse, and begin our calculation at peak power to observe the short-term stability of the crater and its effect on absorption. The postulated initial density profile is shown in Fig. 1. In this figure the laser is incident from the right. The horizontal axis r is the laser axis (an axis of rotational symmetry). The vertical axis is the polar angle θ measured in radians. A super-Gaussian

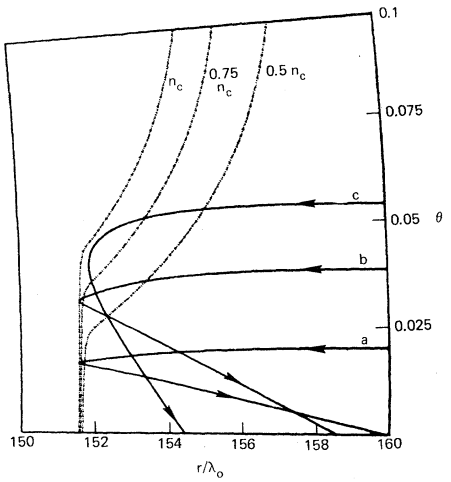

FIG. 1. Contour plot of the initial plasma density. Also shown are numerical solutions for trajectories of three typical rays, rays a–c. The steepened plasma density scale length on the laser axis ($\theta = 0$) is $k_0L = 1$ while far off axis ($\theta = 0.1$) the unsteepened scale length is $k_0L = 24$. Approximately 90% of the incident power is inside ray c.

$\{I=I_0\exp[-(\theta/\theta_0)^4]\}$ laser beam of peak intensity $I_0=3\times10^{15}$ W/cm^2 is focused by an $f/10$ lens onto the rear wall of the crater. The width of the crater corresponds to the diffraction-limited focal-spot size of about 20 μm (Nd light). The average electron temperature is 3.5 keV corresponding to $v_0/v_e=0.6$, where $v_0=eE_0/m\omega_0$ is the electron quiver velocity in the vacuum field. Inverse-bremsstrahlung absorption is negligible in this example. We chose the constant term in the viscosity to give $\omega_i/\omega_r\approx 0.25$ for the ion waves generated by the Brillouin instability ($k\approx 2k_0$). This value of the damping corresponds to a temperature ratio of $T_e/T_i\approx 2$, and effectively saturates Brillouin at a low enough level to be unimportant. We assume a uniform (in θ) plasma flow velocity of $v_i=0.5C_s$ at the inner radial boundary; here C_s is the sound velocity.

The critical surface at the rear of the crater is initially smooth and the density gradient very steep so that one might expect only minimal absorption of the normally incident light, perhaps a few percent. However, the calculated absorption for this initial configuration is about 17%. This enhanced absorption fraction may be understood by an examination of some typical ray trajectories, shown in Fig. 1. The walls of the crater guide the outermost rays (ray c) to propagate nearly parallel to the critical surface. Consequently these rays, which can carry a substantial portion of the total power, are reasonably absorbed with great efficiency. Even rays closer to the center of the crater (rays a and b) are refracted enough to reach the critical surface with an effective angle of incidence of 10°–20°. Accounting for the fact that only half the rays, on the average, have the correct polarization for this enhanced resonant absorption, and using the steepened density scale length $k_0L\sim 1$ we estimate than an energy-averaged refraction of about 25 is sufficient to give the calculated absorption efficiency of 17%. This estimate is certainly reasonable for the trajectories of Fig. 1.

As the calculation proceeds, the initial density profile evolves toward a self-consistent steady state with the incident laser light. Several additional effects due to the hydrodynamic response of the plasma increase absorption still further. Figure 2 shows the critical surface after 372 laser periods (about 15 ps scaled to an average ion mass of $6m_p$). As expected the critical surface becomes rippled. In addition to the rippling, however, there are several effects evident which arise solely due to the finite size of the focal

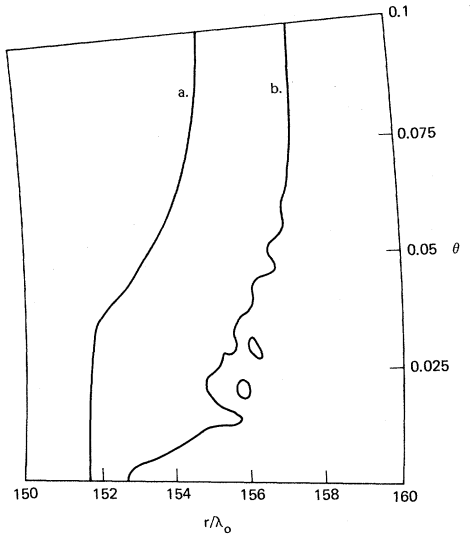

FIG. 2. Critical surface contours (*a*) initial and (*b*) after 372 laser periods.

spot. First, the plasma has expanded around the laser beam making the critical surface more concave, and hence, more oblique to the incident light. A crude estimate from the figure gives about 20° for the average angle between the critical surface contour and the laser axis. Second, the increased depth of the crater increases its self-focusing effect. In fact, the intensity on the laser axis is about an order of magnitude larger than the nominally incident 3×10^{15} W/cm^2. As a result, the critical surface is severely indented there. All of these effects act to increase resonant absorption, so that the time-averaged absorption for this example is about 40%. The scattered light distribution reaches out to about 45°.

Our model has several important limitations. For large focal spots or low intensities, electron conduction may not be sufficient to keep the underdense plasma isothermal. If the plasma near the edge of the beam is relatively cold, then plasma expansion around the beam will be reduced and the resulting crater will not be as pronounced as in the example calculation.

Crater formation is also determined in part by the uniformity of plasma flow into the critical region. For example, if the radial flow velocity is highly peaked on the laser axis, a crater does not form. In theory this plasma-flow boundary condition should be self-consistently determined through detailed considerations of heat transport into the ablation region. However, here we have assumed the simplest possible boundary condi-

tion: uniform subsonic flow.

The requirement of a finite viscosity in the fluid equations introduces some uncertainty into our calculations since it affects the amplitude and wavelength of critical surface ripples and the level of stimulated scattering. The general characteristics of the calculations, however, are fairly constant for reasonable values of the viscosity. Finally, our model neglects dc magnetic fields which may increase, or in some cases, diminish absorption.[8]

In conclusion, we find using a wave-optics–hydrodynamics model that the effects of a finite focal-spot size can significantly increase the absorption of laser light by a plasma. In particular a large crater may form, producing a convex critical surface, refraction of the incident light, and therefore enhanced resonant absorption.

The authors wish to acknowledge valuable discussions with D. Attwood, J. Erkkila, K. Estabrook, W. Kruer, C. Max, and J. J. Thomson. This work was performed under the auspices of the U. S. Department of Energy by the Lawrence Livermore Laboratory under Contract No. W-7405-Eng-48.

[1]D. W. Forslund, J. M. Kindel, K. Lee, E. L. Lindman, and R. L. Morse, Phys. Rev. A 11, 679 (1975).
[2]K. G. Estabrook, E. J. Valeo, and W. L. Kruer, Phys. Fluids 18, 1151 (1975).
[3]D. T. Attwood, D. W. Sweeney, J. M. Auerbach, and P. H. Y. Lee, Phys. Rev. Lett. 40, 184 (1978).
[4]E. J. Valeo and K. G. Estabrook, Phys. Rev. Lett. 34, 1008 (1975).
[5]K. R. Manes, V. C. Rupert, J. M. Auerbach, P. H. Y. Lee, and J. E. Swain, Phys. Rev. Lett. 39, 281 (1977).
[6]B. H. Ripin, Appl. Phys. Lett. 30, 134 (1977).
[7]W. L. Kruer and K. G. Estabrook, Phys. Fluids 20, 1688 (1977).
[8]W. Woo, K. G. Estabrook, and J. S. DeGroot, Phys. Rev. Lett. 40, 1094 (1978).
[9]R. J. Faehl and W. L. Kruer, Phys. Fluids 20, 55 (1977).
[10]W. M. Manheimer, Phys. Fluids 20, 265 (1977); W. M. Manheimer, D. G. Colombant, and B. H. Ripin, Phys. Rev. Lett. 38, 1135 (1977).
[11]J. H. Erkkila, Ph.D. thesis, University of California Lawrence Livermore Laboratory Report No. UCRL-51914, 1975 (unpublished).
[12]J. J. Thomson, C. E. Max, J. Erkkila, and J. E. Tull, Phys. Rev. Lett. 35, 663 (1975).
[13]E. L. Lindman, J. Comput. Phys. 18, 66 (1975).

Texture Transformation and Anisotropic Heat Flow in ^{3}He-A

R. L. Kleinberg[a]
Department of Physics, University of California, San Diego, La Jolla, California 92093
(Received 31 October 1978)

Observations are presented that are consistent with the presence of helical textures in ^{3}He-A close to the transition temperature. The discovery of anisotropy in the heat flow is also reported.

I have made measurements which may support the existence of helical textures in ^{3}He-A very near to the transition temperature. While the existence of this texture has recently been the subject of intense theoretical investigation,[1,2] the present work provides the first experimental information. Moreover I have discovered anisotropy in the heat transport, which may shed light on the fluid mechanics of ^{3}He-A in thermal counterflow.

The apparatus, described in detail elsewhere,[3] consisted of two 5-MHz fundamental X-cut quartz sound transducers separated by quartz bars. The resulting flow channel was 0.1 cm × 1.0 cm × 1.3 cm long. A magnetic field perpendicular to the direction of sound propagation could be applied. Above the transducers a short length of resistive wire served as a heater to drive a counterflow[4] along the field axis; some heat also entered the helium laterally from the sound transducers. A cerium-magnesium-nitrate–based thermometer, calibrated on the line of superfluid-to-normal transitions,[5] was used to measure the temperature above the flow channel. A second cerium-magnesium-nitrate–based thermometer monitored the temperature of the main cooling salt, located below the channel. The pressure was 24.3 bars.

The measurement procedure consisted of dissipating a constant power in the heater and increasing or decreasing the magnetic field while observing the attenuation of 15-MHz sound. Ramping rates were 0.1 G/s or less. Sample experimental data are displayed in Fig. 1. The solid curve was traced out on an X-Y recorder as the magnetic field increased with time; $1-T/T_c=0.0239$. The characteristic magnetic field is $H_c \equiv [\lambda_D/(\chi_N-\chi_d)]^{1/2} \approx 20$ G; χ_d and χ_N are the magnetic sus-